LBL--25807

DE89 002669

RF and Space-Charge Effects in Laser-Driven RF Electron Guns

Kwang-Je Kim
Accelerator and Fusion Research Division
Lawrence Berkeley Laboratory
University of California
Berkeley, CA 94720

September 23, 1988

Abstract

The evolution of the electron-beam phase space distribution in laser-driven RF guns is studied by taking into account both the time variation of the RF field and space-charge effects. In particular, simple formulas are derived for the transverse and longitudinal emittances at the exit of the gun. The results are compared and found to agree well with those from simulation.

1 Introduction

Laser-driven rf electron guns[1] are potential sources of high-current, low-emittance, short bunch-length electron beams, which are required for many advanced accelerator applications, such as free-electron lasers and injectors for high-energy machines. In such guns the design of which was pioneered at los Alamos National Laboratory[1] and is currently being developed at several other laboratories[2,3,4], a high-power laser beam illuminates a photocathode surface placed on an end wall of an rf cavity. The emitted electrons are accelerated immediately to a relativistic energy by the strong rf field in the cavity. The main advantages of this type of gun are that the time structure of the electron beam is controlled by the laser, eliminating the need for bunchers, and that the electric field in rf cavities can be made very strong, so that the degrading effects due to space-charge repulsion can be minimized. In this paper, we analyze the beam dynamics in the rf cavities to obtain the expressions for the transverse and longitudinal emittances of the electron beams emerging from laser-driven rf guns.

A study of electron-beam dynamics in rf guns needs to take into account several effects, such as those due to the time variation of the rf field over the duration of the acceleration period and over the duration of the electron pulse and those due to the space-charge repulsion. A rigorous analysis of these effects is probably too complicated to be useful. The goal in this paper is to obtain approximate and simple expressions that retain the main physical effects.

In Section 2 we study the rf acceleration process. We simplify the calcu-

lation by assuming that only a single standing-wave component is present. However, contrary to what is done for long linear accelerators[5], we do not neglect the contribution from the reflected wave. We solve the rf acceleration equation approximately after noting that the variation of the rf phase $\phi = \omega t - kz + \phi_0$ is significant only at the beginning of the acceleration period. The result agrees reasonably well with exact calculations. Because of the time-variation of the rf field, the electron distribution occupies curved regions in phase-space. We calculate the longitudinal emittance associated with this effect.

In Section 3 we consider the effects of the rf acceleration on transverse dynamics. Given that the longitudinal electric field is uniform in the transverse direction, the expression for the transverse force is uniquely determined from Maxwell's equations. The transverse momentum imparted to an electron is obtained by assuming that the electron's transverse coordinates remain constant during acceleration by the rf field. With this approximation, a net transverse momentum transfer to electrons occurs only in the vicinity of the cavity exit. We calculate the transverse emittance which arises from the fact that electrons at different longitudinal positions near the exit receive different transverse kicks due to the variation of the rf field.

In Section 4 we calculate the transverse and the longitudinal emittances resulting from the space-charge effects. We simplify the calculation by assuming that all electrons move with identical velocity, so that the space-charge force is purely electrostatic in the frame of reference that moves with the electrons. A further simplification is achieved by noting that the influ-

ence of the space-charge force is weighted by a factor $1/\gamma^2\beta$, which heavily emphasizes the region of the cavity near the cathode where the electrons are still non-relativisitic.

Section 5 contains further discussions and conclusions. First, the paper is summarized by recapitulating the main formulas derived therein. Then the results of the analytical calculations are compared with those from numerical simulation. The agreement is found to be satisfactory. Finally, we conclude by listing some of the effects not discussed in the paper.

Appendix A contains a discussion of the scaling behavior for the electrostatic field in the limit where the aspect ratio of the charge distribution either vanishes or becomes large. An understanding of the scaling behavior is important for the derivation of Section 4. In the text, the shape of the charge distribution was assumed to be Gaussian for the purpose of explicit calculations. In Appendix B, we list the relevant formulas for the case where the charge distribution is uniform in a cylinder. Finally, Appendix C contains a discussion of the correlation between the space-charge and the rf effects. It is found that the correlation is not negligible for transverse emittance.

2 RF Acceleration and Longitudinal Phase Space

2.1 RF Acceleration

Electrons generated at the cathode are accelerated by the rf field in a cavity. The electric field along the axis will be assumed to be of the following simple

form:

$$E_z = E_0 \cos kz \sin(\omega t + \phi_0) \quad . \tag{1}$$

Here E_0 is the peak accelerating field, λ is the rf wavelength, $k = 2\pi/\lambda$, c is the velocity of light, $\omega = ck$, and ϕ_0 is the rf phase as the particle leaves the cathode surface $z = 0$ at $t = 0$. The field given by Eq.(1) can be considered to be produced by a sequence of rf cells operating in the π-mode[2]. The first cell is really a half cell bounded at one side by the cathode. The coordinates for the entrance and exit of the $(\frac{1}{2} + n)$th cell are $z = (n - 1/2)\lambda/2$ and $z = (n + 1/2)\lambda/2$, respectively. See Fig. (1).

It is convenient to introduce the following quantity

$$\phi = \omega t - kz + \phi_0 = k \int_0^z \left(\frac{\gamma}{\sqrt{\gamma^2 - 1}} - 1 \right) dz + \phi_0 \quad . \tag{2}$$

Here

$$\frac{\gamma}{\sqrt{\gamma^2 - 1}} = 1/\beta = \left(\frac{1}{c} \frac{dz}{dt} \right)^{-1} \quad . \tag{3}$$

As usual, γ is the electron's relativistic energy divided by the rest energy mc^2, m being the electron mass. We have

$$\frac{d\gamma}{dz} = \frac{eE_0}{2mc^2} [\sin(\phi) + \sin(\varphi + 2kz)] \quad . \tag{4}$$

The rf acceleration in the cavity is completely determined by the pair of equations (2) and (4). We assume that electrons leave the cathode with no kinetic energy, thus $\gamma = 1$ at $z = 0$. Equations (2) and (4) are often solved by neglecting the second term in Eq.(4), which represents the backward-propagating wave[5]. Such an approximation is valid for electrons in long linear accelerators, where the effect of the reflected wave averages to zero. In our present case, this approximation is not adequate.

To obtain a more appropriate approximation, we first note that the integrand in Eq.(2) is significantly larger than zero only near the cathode surface where the electrons are still non-relativistic. In that region, Eq.(4) may also be replaced by

$$\frac{d\gamma}{dz} \approx \frac{eE_0}{mc^2} \sin\phi_0 \quad . \tag{4.a}$$

From this, we obtain an approximate expression $\tilde{\gamma}$ for γ

$$\tilde{\gamma} = 1 + 2\alpha \sin(\phi_0) kz \quad , \tag{5}$$

where

$$\alpha = \frac{eE_0}{2mc^2 k} \tag{6}$$

is a dimensionless parameter representing the strength of the accelerating field. With the use of (4-a), Eq.(2) can be integrated with the result

$$\phi = \frac{1}{2\alpha \sin\phi_0} \left[\sqrt{\tilde{\gamma}^2 - 1} - (\tilde{\gamma} - 1) \right] + \phi_0 \quad . \tag{7}$$

We now insert Eq.(7) into Eq.(4) and integrate the latter for a better approximation of γ. In so doing, we neglect the variation of ϕ with z. The result is

$$\gamma = 1 + \alpha \left[kz \sin\phi + \frac{1}{2}(\cos\phi - \cos(\phi + 2kz)) \right] \quad . \tag{8}$$

The approximate solutions (7) and (8) of Eqs. (2) and (4) are compared with the exact solution in Figs. (2) and (3) for several cases with $\alpha = 1$ and different values of ϕ_0. The agreement is good for γ [Fig.(2)]. For ϕ [see Fig.(3)], the agreement is fair provided that ϕ_0 is not too small. A better approximation to ϕ can be obtained by inserting Eq.(8), in which ϕ is given

by Eq.(7), into Eq.(2), and integrating the latter. However, this cannot be done analytically, and we will not pursue this approach further in this paper.

From Eq.(7), we see that the phase ϕ has the asymptotic value

$$\phi \to \phi_\infty = \frac{1}{2\alpha \sin\phi_0} + \phi_0 \quad . \tag{9}$$

We will show later that the transverse emittance is minimized when ϕ_∞ is $\pi/2$. The initial phase ϕ_0 should then be chosen such that

$$\left(\frac{\pi}{2} - \phi_0\right) \sin\phi_0 = \frac{1}{2\alpha} \quad . \tag{10}$$

2.2 RF Effects on Longitudinal Phase Space Distribution

The spread in the phase $\Delta\phi$ is related to the spread of the longitudinal position by $\Delta\phi = -k\Delta z$. Therefore, particles with positive $\Delta\phi$ are located in the trailing part of the electron bunch relative to those with negative $\Delta\phi$. The longitudinal phase-space is characterized by the pair (z, p_z), where

$$p_z = \beta\gamma \tag{11}$$

is the dimensionless longitudinal momentum. After acceleration, $\beta \approx 1$ so that $p_z \approx \gamma$.

From Eq.(9), we find the asymptotic bunch compression factor

$$\frac{\Delta\phi_\infty}{\Delta\phi_0} = 1 - \frac{\cos\phi_0}{2\alpha \sin^2\phi_0} \quad . \tag{12}$$

Thus bunches will in general be compressed in length during the acceleration process. When $2\alpha \sin^2\phi_0 \leq \cos\phi_0$, Eq.(12) predicts that the relative positions of particles in z will reverse. However, this reversal is a result of

the approximation used in deriving Eq.(9), which becomes poor for small values of ϕ_0. A numerical solution does not show such a reversal. The rf effect on (ϕ, γ) phase space can be derived from Eq.(8), which we have seen [in Fig.(2)] to agree well with exact results[6]. First, we consider the phase-space distribution at the end of the $(n+1/2)$th cavity, where $z = (2n+1)\lambda/4$ and thus

$$\gamma = 1 + \alpha[(n + 1/2)\pi \sin\phi + \cos\phi] \quad . \tag{13}$$

As remarked earlier, we are interested in ϕ when it is about $\pi/2$. The shape of the $\phi - \gamma$ distribution would look like Fig.(4a) when the second term in Eq.(13) is dominant, while it would look like Fig. (4b) when the first term is dominant. In the middle of the $(n + 1/2)$th cavity, $z = n\lambda/2$, so Eq.(8) becomes $\gamma = \pi n\ \alpha \sin\phi + 1$. Thus the phase space distribution around $\phi = \pi/2$ will always look like Fig.(4b).

We write

$$p_z = \langle p \rangle + \Delta p_z, \qquad z = \langle z \rangle + \Delta z \quad , \tag{14}$$

where $\langle p_z \rangle$ and $\langle z \rangle$ are the average values of p and z, respectively. The longitudinal emittance ϵ_z will be defined as[7]

$$\epsilon_z = \sqrt{\langle(\Delta p_z)^2\rangle\langle(\Delta z)^2\rangle - \langle \Delta p\rangle^2\langle \Delta z\rangle^2} = \frac{1}{k}\sqrt{\langle(\Delta p_z)^2\rangle\langle(\Delta \phi)^2\rangle - \langle \Delta p\rangle^2\langle \Delta \phi\rangle^2} \quad , \tag{15}$$

where the angular brackets represent taking the average values.

We assume that electrons are relativistic at the end of the $(n + 1/2)$th cavity, thus p can be replaced by γ in Eq.(15). From Eq.(13) we obtain

$$\langle\gamma\rangle + \Delta\gamma = 1 + \alpha[(n + 1/2)\pi \sin(\langle\phi\rangle + \Delta\phi) + \cos(\langle\phi\rangle + \Delta\phi)] \quad . \tag{16}$$

Setting $\langle\phi\rangle = 90^o$ to minimize the transverse emittance(see Section 3), we obtain by expanding Eq. (16)

$$\Delta\gamma = -\alpha\Delta\phi - \frac{1}{2}(\gamma_f - 1)(\Delta\phi)^2 + \frac{\alpha}{3!}(\Delta\phi)^3 + \cdots \quad , \tag{17}$$

where γ_f is the value of $\langle\gamma\rangle$ at the cavity exit. Introducing the rms quantities

$$\sigma_{\Delta\gamma} = \langle(\Delta\gamma)^2\rangle^{1/2}, \qquad \sigma_\phi = k\sigma_z = \langle(\Delta\phi)^2\rangle^{1/2},$$

we obtain from Eq. (17)

$$\sigma_{\Delta\gamma} = \alpha\sigma_\phi = \alpha k\sigma_z \quad . \tag{18}$$

Inserting Eq.(17) into Eq.(15) ($\Delta p \approx \Delta\gamma$), we obtain ϵ_z in the lowest order in $\Delta\phi$

$$\epsilon_z^{rf} = \frac{1}{k}(\gamma_f - 1)\sqrt{\langle(\Delta\phi)^4\rangle\langle(\Delta\phi)^2\rangle} \quad . \tag{19}$$

The superscript rf refers to the contribution of the time variation of the rf field. There is also a contribution from the space-charge effects, which will be considered later. The terms involving the first and the third terms in Eq.(17) cancel and do not appear in Eq.(19). For a Gaussian distribution, Eq.(19) becomes

$$\epsilon_z^{rf} = \sqrt{3}(\gamma_f - 1)\,k^2\sigma_z^3 \tag{20}$$

3 RF Effects in Transverse Phase Space

Let the longitudinal electric field E_z be a function of only z and t and be independent of the transverse coordinates r (radius) and θ (angle). Assuming that the fields are independent of θ, we determine from Maxwell's equations

that[5]

$$E_r = -\frac{r}{2}\frac{\partial}{\partial z}E_z, \text{ and } cB_\theta = \frac{r}{2c}\frac{\partial}{\partial t}E_z \quad . \tag{21}$$

The radial force acting on an electron is given by

$$F_r = e(E_r - \beta c B_\theta) \quad . \tag{22}$$

We now assume that E_z is given by the somewhat more general expression than Eq.(1)

$$E_z = E(z)\cos kz \sin(\omega t + \phi_0) \quad . \tag{23}$$

One can show from the above equations that

$$F_r = er\left\{-\frac{1}{2c}\frac{d}{dt}\left(E(z)\sin kz\cos(\omega t+\phi_0)\right) - \frac{1}{2}\left(\frac{d}{dz}E(z)\right)\cos kz\sin(\omega t+\phi_0)\right. \quad .$$
$$\left. + \frac{\beta}{2}\left(\frac{d}{dz}E(z)\right)\sin kz\cos(\omega t+\phi_0)\right\} \quad . \tag{24}$$

The equation describing the radial motion is

$$\frac{dp_r}{dt} = \frac{1}{mc}F_r \quad . \tag{25}$$

Here p_r is the dimensionless radial momentum

$$p_r = \gamma\frac{1}{c}\frac{dr}{dt} \tag{26}$$

We integrate Eq.(25) with respect to t to obtain p_r. In doing so, we assume that the transverse deflection is small so that the radius r can be regarded as constant. Since the first term in Eq.(25) [with F_r given by Eq.(24)] is a total time derivative of an expression that vanishes on the cathode surface and at the outside of the cavity exit, its integral vanishes. The contribution of the second and third terms comes only from the region where $dE(z)/dz$ is

non-vanishing, i.e, near the cavity exit. Thus the net momentum transfer in our approximation occurs only during the short interval that the electrons cross the boundary between the cavity and the field-free region. We take $E(z)$ to be of the form

$$E(z) = \theta(z_f - z)E_0 \quad , \tag{27}$$

where θ is the step function and $z = z_f$ is the coordinate of the exit of the cavity. Thus, the second and third terms in Eq.(24) become delta functions and one obtains

$$p_r = p_{r_0} + \alpha k r \left[\beta \cos kz_f \sin(\omega t + \phi_0) - \sin kz_f \cos(\omega t + \phi_0)\right], \tag{28}$$

where α was introduced in Eq.(6). In the following, we assume $\beta_r = 0$ at $t = 0$, thus dropping the first term of Eq.(28). Since $\beta \approx 1$ near the cavity exit, Eq.(28) becomes

$$p_r = \alpha k r \sin\phi \quad . \tag{29}$$

Here ϕ is the rf phase at the exit of the cavity. Rewriting Eq.(29) in cartesian coordinates, we obtain

$$p_x \equiv \beta\gamma x' = (\alpha k \sin\phi)x \quad , \tag{30}$$

where $x' = dx/dz$. The phase-space distribution given by Eq.(30) therefore consists of a collection of lines with different slopes corresponding to different ϕ, as illustrated in Fig.(5).

The normalized transverse emittance is[7]

$$\epsilon_x = \sqrt{\langle p_x^2\rangle\langle x^2\rangle - \overline{\langle p_x x\rangle^2}} \quad . \tag{31}$$

From Eqs.(30) and (31) we obtain

$$\epsilon_x^{rf} = \alpha k \langle x^2 \rangle \sqrt{\langle \sin^2 \phi \rangle - \langle \sin \phi \rangle^2} \quad . \tag{32}$$

Writing $\phi = \langle \phi \rangle + \Delta\phi$, and assuming that $\Delta\phi$ is small and symmetrically distributed, one obtains

$$\epsilon_x^{rf} = \alpha k \langle x^2 \rangle \sqrt{\left[\langle (\Delta\phi)^2 \rangle - \frac{1}{3} \langle (\Delta\phi)^4 \rangle \right] \cos^2 \langle \phi \rangle + \frac{1}{4} \left[\langle (\Delta\phi)^4 \rangle - \langle (\Delta\phi)^2 \rangle^2 \right] \sin^2 \langle \phi \rangle} \quad .$$

This expression is minimized when $\langle \phi \rangle = 90°$ with the value

$$\epsilon_x^{rf} = \alpha k \frac{\langle x^2 \rangle}{2} \sqrt{\langle (\Delta\phi)^4 \rangle - \langle (\Delta\phi)^2 \rangle^2} \; ; \langle \phi \rangle = 90° \tag{33}$$

Away from the minimum, we have

$$\epsilon_x^{rf} \sim \alpha k \langle x^2 \rangle \sqrt{\langle (\Delta\phi)^2 \rangle} \, |\cos \langle \phi \rangle| \; ; \langle \phi \rangle \neq 90° \; . \tag{34}$$

If the distribution in $\Delta\phi$ is Gaussian, Eq.(33) becomes

$$\epsilon_x^{rf} = \frac{\alpha k \langle x^2 \rangle \sigma_\phi{}^2}{\sqrt{2}}, \quad \langle \phi \rangle = 90° \; . \tag{35}$$

In view of Eqs. (29) and (30), the transverse momentum is maximum when $\langle \phi \rangle = 90°$, i.e., when the emittance is minimum. The rms angular divergence $\sigma_{x'}$ is in that case given by

$$\sigma_{x'} = \frac{\alpha}{\gamma} k \sigma_x \quad . \tag{36}$$

Thus it usually will be necessary to focus the beam immediately after leaving the cavity.

4 Space Charge Effects on Beam Emittance

4.1 General charge distribution

A repulsive force attributable to space charge causes the emittance to increase. To study this effect, we assume that all electrons are moving with the same velocity, v, in the z-direction. In the reference frame moving with the electrons, the electromagnetic interaction is completely described by a purely electrostatic field $\mathbf{E}'$. The field components in the laboratory frame which give rise to the x- and z-components of the force are given by the Lorentz transformation

$$E_x = \gamma E'_x, \quad B_y = \gamma \frac{v}{c^2} E'_x \ , \quad E_z = E'_z$$

Here, B_y is the magnetic field. The components of the force are

$$F_x = e(E_x - vB_y) = \frac{e}{\gamma} E'_x \quad , \quad F_z = eE'_z \quad . \tag{37}$$

In the following, we assume the charge distribution to be cylindrically symmetric, so that we do not need to consider F_y separately.

Let us now consider the behavior of $\mathbf{F}$ as γ becomes large. The field E' is a function of γ since the bunch dimensions in the moving frame, d'_x in the transverse direction and d'_z in the longitudinal direction, are related to the corresponding bunch dimensions in the laboratory frame d_x and d_z by

$$d'_x = d_x \ , \quad d'_z = \gamma d_z \ ; \tag{38}$$

that is, the bunch in the moving frame appears to be elongated by a factor γ. In Appendix A, we have summarized the behavior of the electric field of

a general, stationary charge distribution in the limits when the aspect ratio $A' = d'_x/d'_z$ becomes either much smaller or much larger than unity. When γ is much larger than the aspect ratio A in the laboratory frame, $A' = A/\gamma$ becomes small. From Eqs. (A.1) and (38) it then follows, for a typical point within the charge distribution,

$$E'_x \sim O(\gamma^{-1}), \quad E'_z \sim O(\gamma^{-2}) \quad \text{for } \gamma \gg A \quad .$$

Here $f \sim O(\gamma^n)$ means that f scales as γ^n times some slowly varying function such as $(\log\gamma)^n$. From these it follows that

$$\mathrm{F} \sim O(\gamma^{-2}) \quad \text{for } \gamma \gg A. \tag{39}$$

For cases where A is much larger than unity, we need to consider also the case $1 \leq \gamma \ll A$. The aspect ratio in the moving frame A' is then much larger than unity, in which case we find from Eq. (A.2) that E'_x and E'_z are both $O(1)$. To summarize these behaviors, it is convenient to write

$$\mathrm{F} = \frac{1}{\gamma^2}\mathrm{f}(\gamma) \quad . \tag{40}$$

The function $\mathrm{f}(\gamma)$ behaves as follows:

$$\mathrm{f}(\gamma) \sim O(1) \quad , \quad \gamma \gg A \quad , \tag{41}$$

$$f_x \sim O(\gamma) \quad \textit{and} \quad f_z(\gamma) \sim O(\gamma^2) \quad , \quad 1 \leq \gamma \ll A \quad . \tag{42}$$

The contribution to the electron's dimensionless momentum due to the space-charge force is given by

$$(p_x, p_y, \Delta p_z) \equiv \mathrm{p} = \frac{1}{mc}\int \mathrm{F}\, dt = \frac{1}{mc^2}\int \frac{1}{\gamma^2\beta}\mathrm{f}(\gamma)\, dz \quad . \tag{43}$$

Let us assume for the time being that $A \leq 1$. From Eq.(41), we see that $\mathbf{f}(\gamma)$ is a slowly varying function of γ. Since the factor $1/\gamma^2\beta$ in the integrand decreases rapidly as the electron accelerates (γ increases from unity), the function $\mathbf{f}(\gamma)$ may be replaced by $\mathbf{f}(1)$. Also, Eq.(4.a) may be used to replace the z-integration by a γ-integration. Thus we obtain

$$\mathbf{p} = \frac{1}{eE_0 \sin\phi_0} \mathbf{f}(1) \int_1^{\gamma_f} \frac{d\gamma}{\gamma^2\beta} \quad . \tag{44}$$

The integration in the above can be done analytically as follows

$$\int_1^{\gamma_f} \frac{d\gamma}{\gamma^2\beta} = \int_1^{\gamma_f} \frac{1}{\sqrt{1-1/\gamma^2}} \frac{1}{\gamma^2}\, d\gamma = \left[\frac{\pi}{2} - \sin^{-1}(\frac{1}{\gamma_f})\right] \quad .$$

For $\gamma_f \gg 1$, the integral becomes $\pi/2$. From Eqs. (37) and (40), we obtain $\mathbf{f}(1) = e\mathbf{E}^{sc}$ where $\mathbf{E}^{sc}$ is the electrostatic field due to the charge distribtion at rest in the laboratory frame. Thus we finally obtain

$$\mathbf{p} = \frac{1}{E_0 \sin\phi_0} \frac{\pi}{2} \mathbf{E}^{sc} \quad . \tag{45}$$

It is convenient to introduce the normalized field $\mathcal{E}$

$$\mathbf{E}^{sc}(x, y, \Delta z) = \frac{n_0}{4\pi\epsilon_0}\ \mathcal{E}(x, y, \Delta z) \quad . \tag{46}$$

Here $(x, y, \Delta z)$ is the position relative to the bunch center. The axial distance of the bunch center to the cathode center is z. In the above, n_0 is the line density at the bunch center, i.e..

$$n_0 = \int \rho(x, y, 0)\, dx\, dy \quad ,$$

where $\rho(x, y, z)$ is the volume density of the charge distribution. The normalized field $\mathcal{E}$ has the dimension of an inverse length. From Eqs.(45), (46),

(15) and (31) we obtain

$$\epsilon_i^{sc} = \frac{\pi}{4}\frac{1}{\alpha k}\frac{1}{\sin\phi_0}\frac{I}{I_A}\mu_i(A)\ ;\ i = x \text{ or } z \quad . \tag{47}$$

Here, α is the dimensionless rf strength parameter introduced in Eq.(6), I is the peak current, $I_A = 4\pi\epsilon_0 mc^3/e = 17{,}000\text{A}$ known as the Alfvén current, and

$$\mu_x(A) = \sqrt{\langle\mathcal{E}_x^2\rangle\langle x^2\rangle - \langle\mathcal{E}_x \cdot x\rangle^2} \ , \tag{48}$$

$$\mu_z(A) = \sqrt{\langle\mathcal{E}_z^2\rangle\langle\Delta z^2\rangle - \langle\mathcal{E}_z \cdot \Delta z\rangle^2} \quad . \tag{49}$$

The dimensionless functions $\mu_x(A)$ and $\mu_z(A)$ will be referred to as the transverse and the longitudinal space-charge factors respectively. The angular brackets in the above represent (as usual) taking the average over the charge distribution. Thus, for example,

$$\langle\mathcal{E}_x^2\rangle = \frac{1}{Q}\int \rho(x,y,\Delta z)\mathcal{E}_x^2(x,y,\Delta z)\,dx\,dy\,d\Delta z \quad ,$$

where Q is the total charge in the bunch.

The space-charge factors, being dimensionless, depend on the details of the charge distribution only through the dimensionless aspect ratio A. From Eqs.(A.1) and (46), it follows that

$$\mathcal{E}_{x,z} \sim \frac{Q}{\epsilon_0 d_{x,z}} O(1), \quad A \to 0 \quad .$$

Thus, the space-charge factors can have at most a logarithmic singularity at $A = 0$:

$$\mu_x(A) \sim O(1)\ , \quad \mu_z(A) \sim O(1) \quad . \tag{50}$$

The limiting behavior of $\mu_j(A)$ as A increases to infinity is as follows:

$$\mu_x(A) \sim O(A^{-1}), \quad \mu_z(A) \sim O(A^{-2}), \quad A \to \infty \quad . \tag{51}$$

In deriving Eq.(47), we have assumed that $A \leq 1$ so that the function $\mathrm{f}(\gamma)$ is slowly varying in γ for all $\gamma \geq 1$. According to Eq.(42), when $A \gg 1$, the function $\mathrm{f}(\gamma)$ in the region $1 \leq \gamma < A$ does not vary slowly with γ. A proper analysis of the space-charge emittance in this case involves integrating Eq.(43) exactly and evaluating emittances according to Eqs. (15) and (31). We have carried out such calculations and found that the result does not differ significantly from those obtained by the approximate calculations; the agreement was better than 50transverse emittance and better than a factor of two for the longitudinal emittances. We will therefore use the approximate formula, Eq.(47), for all values of A. The derivation leading to Eq.(47), which is the main result of this section, is a refinement of a previous calculation[8] in that the variation of the electron energy in the cavity is correctly taken into account.

4.2 Gaussian charge distribution

We apply the general discussion in the above to the case where the charge density is given by

$$\rho(x, y, \Delta z) = \rho_0 e^{-\frac{1}{2}\left[\frac{x^2+y^2}{\sigma_x^2} + \frac{\Delta z^2}{\sigma_z^2}\right]} \quad , \tag{52}$$

where ρ_0 is the charge density at the bunch center, and σ_x (σ_z) is the rms beam size in the x (z) direction. Using $n_0 = 2\pi\rho_0\sigma_x^2$, we obtain for the

space-charge field[9]

$$\mathcal{E}_x(x,y,\Delta z) = \frac{x}{\sigma_x^2}\int_0^\infty d\zeta\, \frac{e^{-\frac{1}{2}\left[\frac{x^2+y^2}{\sigma_x^2(1+\zeta)}+\frac{\Delta z^2}{\sigma_z^2(1+A^2\zeta)}\right]}}{(1+\zeta)^2(1+A^2\zeta)^{1/2}} \quad , \tag{53}$$

$$\mathcal{E}_z(x,y,\Delta z) = \frac{\Delta z}{\sigma_z^2}\int_0^\infty d\zeta\, \frac{e^{-\frac{1}{2}\left[\frac{(x^2+y^2)A^2}{\sigma_x^2(\zeta+A^2)}+\frac{\Delta z^2}{\sigma_z^2(1+\zeta)}\right]}}{(1+\zeta)^{3/2}(A^2+\zeta)} \quad . \tag{54}$$

Here A is the aspect ratio

$$A = \frac{\sigma_x}{\sigma_z} \quad . \tag{55}$$

Inserting Eqs. (53) and (54) into Eqs. (48) and (49), we obtain

$$\begin{aligned}\mu_x^2(A) = \int_0^\infty d\zeta_1 \int_0^\infty d\zeta_2 \Bigg\{ & \frac{1}{[(1+\zeta_1)(1+\zeta_2)+2+\zeta_1+\zeta_2]^2} \\ & \times \frac{1}{[(1+\zeta_1 A^2)(1+\zeta_2 A^2)+2+(\zeta_1+\zeta_2)A^2]^{1/2}} \Bigg\} \\ & - \left[\int_0^\infty d\zeta\, \frac{1}{(2+\zeta)^2(2+\zeta A^2)^{1/2}}\right]^2\end{aligned} \tag{56}$$

$$\begin{aligned}\mu_z^2(A) = \int_0^\infty d\zeta_1 \int_0^\infty d\zeta_2 \Bigg\{ & \frac{1}{[(A^2+\zeta_1)(A^2+\zeta_2)+2A^4+(\zeta_1+\zeta_2)A^2]} \\ & \times \frac{1}{[(1+\zeta_1)(1+\zeta_2)+2+(\zeta_1+\zeta_2)]^{3/2}} \Bigg\} \\ & - \left[\int_0^\infty d\zeta\, \frac{1}{(2A^2+\zeta)(2+\zeta)^{3/2}}\right]^2 \quad .\end{aligned} \tag{57}$$

In the limit $A \to 0$, $\mu_x(A)$ approaches the value

$$\mu_x(0) = \sqrt{\frac{1}{\sqrt{3}}\log\frac{4}{3} - \frac{1}{8}} \approx 0.203 \quad ,$$

and $\mu_z(A)$ diverges as $(\log A)^2$. These behaviors are consistent with Eq.(50). Also, it is easy to verify that Eq.(51) is satisfied.

When Eq.(60) is evaluated numerically, the result can be approximated by the following simple expression

$$\mu_{xa}(A) = \frac{1}{3A+5} \quad . \tag{58}$$

Both $\mu_x(A)$ and $\mu_{xa}(A)$ are plotted in Fig.(6).

Similarly, we plot in Fig.(7) the function $\mu_z(A)$. It can be approximated by

$$\mu_{za}(A) = \frac{1.1}{1+4.5A+2.9A^2}. \tag{59}$$

The calculation of the space-charge factors in the case where the charge is uniformly distributed in a cylinder is considered in Appendix B.

5 Summary, Comparison and Concluding Remarks

5.1 Summary of the Formulas

The paper can be summarized by recapitulating the main formulas as follows: first, we have introduced the dimensionless parameter characterizing the rf field strength by

$$\alpha = \frac{eE_0}{2mc^2k} \quad . \tag{6}$$

The expressions for various quantities at the exit of an $\left(\frac{1}{2}+n\right)$-cell are as follows:

5.1.1 The phase and energy of the electron

$$\phi_f = \phi_0 + \frac{1}{2\alpha \sin\phi_0} \quad , \tag{9}$$

$$\gamma = 1 + \alpha\,[(n + 1/2)\pi \sin\phi + \cos\phi] \quad . \qquad (13)$$

To minimize the transverse emittance and also to obtain maximum acceleration, one would normally choose $\phi_f = 90°$. We assume that this is case in the following. Equation (9) determines the initial phase ϕ_0.

5.1.2 The rms energy spread $\sigma_{\Delta\gamma}$ and the angular divergence

$$\sigma_{\Delta\gamma} = \alpha k \sigma_z \quad , \qquad (18)$$

$$\sigma_{x'} = \frac{1}{\gamma_f} \alpha k \sigma_x \quad . \qquad (36)$$

Here σ_x and σ_z/c are the rms width and length in time of the laser pulse.

5.1.3 The emittances due to the rf effect are

$$\epsilon_x^{rf} = \frac{\alpha k^3 \sigma_x^2 \sigma_z^2}{\sqrt{2}} \quad , \qquad (35)$$

$$\epsilon_z^{rf} = \sqrt{3}(\gamma_f - 1) k^2 \sigma_z^3 \quad . \qquad (20)$$

5.1.4 The emittances due to the space-charge effect

$$\epsilon_{x,z}^{sc} = \frac{\pi}{4} \frac{1}{\alpha k} \frac{1}{\sin\phi_0} \frac{I}{I_A} \mu_{x,z}(A) \quad . \qquad (47)$$

Here $I_A = 17000$ Amp and I is the peak current. The transverse and the longitudinal space charge factors, μ_x and μ_z, are plotted in Figs. (6) and (7).

The electron distribution is assumed to be Gaussian in the above. Appendix B gives results relevant for a uniform distribution (a cylinder).

5.2 Comparison with Simulation

We consider the $(\frac{1}{2}+1)$-cell gun under construction at Brookhaven National Laboratory and compare the analysis of this paper with the numerical simulation by McDonald[2], hereafter referred to as KM. The gun parameters are

$$eE_0 = 100MV/m\,, \quad \lambda = 10.5cm.$$

The dimensionless rf strength α [Eq. (6)] corresponding to this case is $\alpha = 1.64$. The optimum initial phase calculated from Eq.(9) by demanding that the final phase ϕ_f be 90° is $\phi_0 = 71°$ as compared to $\phi_0 = 68°$ in KM. The final γ calculated from Eq.(13) by setting $n = 1$, $\phi = 90°$, and the above value of α is $\gamma_f = 8.7$ as compared to $\gamma_f = 9.2$ in KM.

The rms bunch length is $\sigma_z = 0.6\ mm$ or $\sigma_\phi = k\sigma_z = 3.6 \times 10^{-2}$. From Eq.(18), the corresponding rms energy spread is $\sigma_E = mc^2\sigma_{\Delta\gamma} = 30$ keV as compared to $\sigma_E = 17$ keV in KM.

The rms beam transverse size is $\sigma_x = 35$mm. From Eq.(36), we obtain the transverse angular divergence at the exit of the gun to be $p_x = \alpha k\sigma_x/\gamma \approx 40$ mrad, which is in rough agreement with Fig.(4) in KM.

The rf contribution to the transverse emittance from Eq.(35) is 1.1 mm-mrad, as compared to 1.4 mm-mrad in KM (Table 1). The transverse space-charge factor corresponding to the aspect ratio $A = 3.5/0.6 \approx 6$ is, from Fig. (6), $\mu_x \sim 4 \times 10^{-2}$. From Eq.(47) and using $I = c \times 1\ nC/\sqrt{2\pi}\ \sigma_z \approx 200A$, we obtain ϵ_x^{sc} =4 mm-mrad, as compared to ϵ_x^{sc} =6.2 mm-mrad obtained by KM.

The longitudinal space-charge factor for $A = 6$ is about 0.01 from Fig.

(8). The quantity ϵ_z^{sc}/γ_f determined from Eq.(47) is about 1×10^{-5} cm. The longitudinal emittance due to the rf effect is about three times larger than the space-charge emittance. The total phase-space area is in rough agreement with the phase-space area indicated by Fig.(5) of KM.

The agreement of our simple theory with the simulation calculation is encouraging. Further comparison is reported in reference (10).

5.3 Further Remarks

In this paper, we have developed an approximate but simple theory of electron beam dynamics in laser-driven rf guns and derived formulas for various physically interesting quantities such as emittances. These formulas should be useful in selecting initial parameters for the design of the gun.

There are several effects which are not taken into account in this simple treatment, such as field non-linearities, higher space harmonics, image-charge effects, etc. The fact that the results of the simple theory agree reasonably well with those of detailed simulation suggests that those effects are small. There are also contributions to the emittances from the photo-emission process at the cathode surface. These contributions, which are easy to incorporate into our expressions, are usually much smaller than those considered in this paper.

Acknowledgements: The author thanks R. Miller, A. Sessler, Y.-J. Chen, K.M. McDonald and S. Chattopadhay for useful discussions. He also thanks B.E. Carlsten for introducing him to the subject of emittance blow-up due to space-charge effects. This work was supported by the Director, Office of Energy Research, Office of Basic Energy Sciences, Materials Sciences Division,

U.S. Department of Energy under Contract No. DE-AC03-76SF00098.

APPENDICES

A Scaling Behavior of the Electrostatic Field for Limiting Charge Distribution

In this Appendix, we derive the scaling behavior of the electric field at typical points inside a stationary charge distribution. The transverse and the longitudinal dimensions of the charge distribution are denoted by $d'_x$and d'_z , respectively. In the limit the aspect ratio $A' = d'_x/d'_z$ (a thin, cigar-shaped distribution) the transverse field E'_x should be of the order $(1/\epsilon_0) \times$ line density$/d'_x$, while the longitudinal field E'_z should be of the order $Q/\epsilon_0/(\text{longitudinal dimension})^2$. Thus

$$E'_x \sim \frac{Q}{\epsilon_0} O\left(\frac{1}{d'_x d'_z}\right) \quad and \; E'_z \sim \frac{Q}{\epsilon_0} O\left(\frac{1}{d'^2_x}\right) \; , A' \to 0. \tag{A.1}$$

In the other limit, where $A \to \infty$, (a thin pancake), E'_z is of the order $(1/\epsilon_0) \times$ surface density while $E'_x \sim /(\text{transverse dimension})^2$. Thus

$$E'_x \sim \frac{Q}{\epsilon_0} O\left(\frac{1}{d'^2_x}\right) \quad \text{and } E'_z \sim \frac{Q}{\epsilon_0} O\left(\frac{1}{d'^2_x}\right) \; , A' \to \infty. \tag{A.2}$$

In the above, $O(1/d'^2_z)$ for example is a quantity of order $1/d'^2_z$, except for a possible logarithmic factor such as $(\log A')^m$, $m =$ an integer.

B Formulas for Uniform Charge Distribution in a Cylinder

The examples treated in the text are based on the Gaussian charge distribution. In this appendix, we list formulas for the case where the charge distribution is uniform in a cylinder of radius a and length L.

The relevant moments for the distribution are

$$\langle x^2 \rangle = \frac{a^2}{4}, \quad \langle (\Delta\phi)^2 \rangle = \frac{k^2 L^2}{12}, \quad \langle (\Delta\phi)^4 \rangle = \frac{k^4 L^4}{80}. \tag{B.1}$$

Using these in Eqs. (19) and (33), we obtain

$$\epsilon_x^{rf} = \frac{\alpha a^2 k^3 L^2}{4\sqrt{6!}} \quad \text{and} \quad \epsilon_z^{rf} = \frac{1}{8\sqrt{15}}(\gamma_f - 1)k^2 L^3 \quad , \tag{B.2}$$

$$\mathcal{E}_x(x,y,z) = \frac{2}{\pi a}\frac{x}{r}\int_0^\pi d\phi \cos\phi \log\left(\frac{R_- - z_-}{R_+ - z_+}\right), \tag{B.3}$$

$$\mathcal{E}_z(x,y,z) = \frac{2}{\pi a^2}\int_0^\pi d\phi \left\{ R_- - R_+ + \sqrt{r^2 + z_+^2} - \sqrt{r^2 + z_-^2} \right.$$

$$\left. + r\cos\phi \log \frac{(-r\cos\phi + \sqrt{r^2 + z_+^2})(a - r\cos\phi + R_-)}{(-r\cos\phi + \sqrt{r^2 + z_-^2})(a - r\cos\phi + R_+)} \right\} \quad . \tag{B.4}$$

Here $r = \sqrt{x^2 + y^2}$ and

$$z_\pm = z \pm L/2 \qquad R_\pm = \sqrt{r^2 + a^2 - 2ra\cos\phi + z_\pm^2} \quad . \tag{B.5}$$

The transverse space charge factor calculated from Eqs. (B.3) and (48) is plotted in Fig.(B.1). The aspect ratio in this case is $A = A/L_1$. It is about $1/A$ times that of the Gaussian case for all A except for $A \to 0$, where it vanishes rapidly. This is because the transverse space-charge field becomes linear in the limit $A \to 0$. The longitudinal space-charge factor for the uniform charge distribution in the cylinder, calculated from Eqs. (B.4) and (49), is plotted in Fig.(B.2). It is about as that of the Gaussian charge distribution for small A but decreases rapidly as A becomes large. Again, this is due to the fact that the longitudinal space-charge field becomes linear in this limit.

C Correlation Between the RF and the Space-Charge Effects

In the text, the contributions to the emittance of the rf effect and the space-charge effect were stated separately. When the magnitudes of these two contributions are comparable, the question arises as to how these individual contributions should be combined to obtain the total emittance. It is tempting to argue that the rf and the space-charge effects are independent and therefore that the total emittance is simply effects are in fact correlated, and the total emittance cannot be separated into two independent parts.

To see this for the transverse case, we write the tota. momentum p_x as

$$p_x = p_x^{rf} + p_x^{sc} , \tag{C.1}$$

where p_x^{rf} and p_x^{sc} are the transverse momentum due to the rf and space-charge effects, respectively. The total emittance can then be written as

$$\epsilon_x = \sqrt{(\epsilon_x^{rf})^2 + (\epsilon_x^{sc})^2 + 2(\epsilon_x^{rf})(\epsilon_x^{sc})^2 \mathcal{J}_x}. \tag{C.2}$$

Here $\mathcal{J}_x$ is a dimensionless paramter characterizing the correlation given by

$$\mathcal{J}_x = \frac{1}{\epsilon_x^{rf}\epsilon_x^{sc}} \left\{ \langle x^2 \rangle \langle p_x^{rf} \cdot p_x^{sc} \rangle - \langle x \cdot p_x^{rf} \rangle \langle x \cdot p_x^{sc} \rangle \right\}. \tag{C.3}$$

Since both p_x^{rf} and p_x^{sc} are unique functions of the position variables, $\mathcal{J}_x$ in the above will not in general vanish. Using the explicit expressions, Eqs. (30) and (45), we find

$$\mathcal{J}_x = \frac{1}{\epsilon_x^{rf}\epsilon_x^{sc}} \frac{\pi}{4} \frac{I}{I_A} \left\{ \langle x^2 \rangle \langle x\xi_x \sin\phi \rangle - \langle x^2 \sin\phi \rangle \langle x\xi_x \rangle \right\} \tag{C.4}$$

Since $\phi = \langle\phi\rangle + \Delta\phi \equiv \langle\phi\rangle - k\Delta z$, we have, for example,

$$\langle \sin\phi x\mathcal{E}_x\rangle \equiv \frac{1}{Q}\int \rho(x,y,\Delta z)\sin(\langle\phi\rangle - k\Delta z)x\mathcal{E}_x(x,y,\Delta z)\,dx\,dy\,d\Delta z \qquad \text{(C.5)}$$

For $\langle\phi\rangle = 90°$, Eq.(C.4) becomes

$$\mathcal{J}_x = \frac{\langle(\Delta\phi)^2\rangle\langle x\mathcal{E}_x\rangle - \langle x\cdot\mathcal{E}_x(\Delta\phi)^2\rangle}{\mu_x(A)\sqrt{\langle(\Delta\phi)^4\rangle - \langle(\Delta\phi)^4\rangle^2}}\,. \qquad \text{(C.6)}$$

For the Gaussian distribution treated in Section 4.b, this becomes

$$\mathcal{J}_x = \frac{1}{\sqrt{2}\mu_x(A)}\int_0^\infty d\zeta \frac{1}{(2+\zeta)^2(2+A^2\zeta)^{3/2}}. \qquad \text{(C.7)}$$

Figure (C.1) gives a plot of $\mathcal{J}_x$ as a function of A. From the figure, we see that the correlation is significant and that

$$0 < \mathcal{J}_x < 1\,. \qquad \text{(C.8)}$$

From Eqs. (C.2) and (C.8) it follows that

$$\sqrt{(\epsilon_x^{rf})^2 + (\epsilon_x^{sc})^2} < \epsilon_x < \epsilon_x^{rf} + \epsilon_x^{sc}\,. \qquad \text{(C.9)}$$

For the longitudinal case, we have expressions similar to Eqs. (C.1), (C.2) and (C.3), except that x's are replaced by z's. Using the expressions for p_z^{rf} and p_z^{sc} given respectively by Eqs. (17) and (45), we obtain

$$\mathcal{J}_z = \frac{\alpha k}{3(\gamma_f - 1)}\frac{\{\langle\Delta z\mathcal{E}_z\rangle\langle(\Delta z)^4\rangle - \langle(\Delta z)^2\rangle\langle(\Delta z)^3\mathcal{E}_z\rangle\}}{\mu_z(A)\sqrt{\langle(\Delta z)^4\rangle\langle(\Delta z)^2\rangle}}. \qquad \text{(C.10)}$$

For the Gaussian distribution considered in Section 4.b, this becomes

$$\mathcal{J}_z = \frac{\sqrt{3}\alpha}{3(\gamma_f - 1)}\sigma_\phi\hat{\mathcal{J}}_z, \qquad \text{(C.11)}$$

where

$$\bar{J}_z = \frac{1}{\mu_z(A)} \int_0^\infty d\zeta \, \frac{1}{(2+\zeta)^{5/2}(2A^2+\zeta)}. \tag{C.12}$$

From Fig. (C.2), we see that $\bar{J}_z$ is large, being about unity for $A \leq 1$. However, the longitudinal correlation is small in general because of the factor $\sigma_\phi = k\sigma_z$ in Eq. (C.11).

References

1. J.S. Fraser et al., "Photocathodes in Accelerator Applications," Proc. 1987 IEEE Particle Accelerator Conference, IEEE Cat. No. 87CH.2387-9, 1705 (March, 1987).

2. K.T. McDonald, "Design of the Laser-Driven RF Electron Gun for the BNL Accelerator Test Facility," Princeton Preprint DOE/ER/3072-43 (March, 1988); submitted to IEEE trans. on Electron Devices.

3. S. Chattopadhay et al., "Conceptual Design of a Bright Electron Injector based on a Laser-Driven Photo-Cathode RF Gun," paper submitted to 1988 Linear Accelerator Conference.

4. H. Chaloupka et al., "A Proposed Super Conducting Photoemission Source of High Brightness," paper submitted to the European Particle Accelerator Conference, Rome, Italy (June 7-11, 1988).

5. See, for example, R.H. Helm and R. Miller, "Particle Dynamics," in *Linear Accelerators*, Ed. by P.M. Lapostolle and A.L. Septier (North-Holland Publ. Co., 1969), p. 115.

6. Actually, Fig.(2) compares Eq.(8), with ϕ replaced by the approximate expression Eq.(7). If one uses the exact ϕ in Eq.(8), the agreement is still good, somewhat better for smaller ϕ_0 and somewhat worse at larger ϕ_0.

7. P.M. Lapostolle, "Possible Emittance Increase Through Filamentation Due to Space Charge in Continuous Beam," IEEE Trans. Nucl. Sci.

18, 1101 (1971).

8. M.E. Jones and B.E. Carlsten, "Space-Charge Induced Emittance Growth in the Transport of High-Brightness Electron Beams," Proc. 1987 IEEE Particle

9. See, for example, E. Keil, "Beam-Beam Interactions in p-p Storage Rings," CERN 77-13, 314 (July, 1977). Accelerator Conference, IEEE Cat. No. 87.CH2387-9, 1319 (March 1987).

10. K.-J. Kim and Y-.J. Chen, "Formulas for RF and Space-Charge Induced Emittances in Laser-Driven RF Guns," paper submitted to 1989 Linear Accelerator Conference.

Figure Captions

Fig.(1) Schematics of the RF laser gun

Fig.(2) Evolution of γ through the RF cavity for the cases $\alpha = 1.0$, $\phi_0 = 70°$ (a) and $\alpha = 1.0$, $\phi_0 = 30°$ (b). The solid lines are the exact solutions, and the dotted lines are the approximate results obtained by inserting Eq.(7) into Eq.(8).

Fig.(3) Evolution of ϕ through the RF cavity for the cases $\alpha = 1.0$, $\phi_0 = 70°$ (a) and $\alpha = 1.0$, $\phi_0 = 30°$ (b). The solid lines are the exact solutions, and the dotted lines are the approximate result given by Eq.(7).

Fig.(4) Schematics showing distortion of the longitudinal phase space due to the RF field

Fig.(5) Electron distribution in transverse phase space due to time-dependent focussing of the RF field

Fig.(6) The transverse space-charge factor $\mu_x(A)$. The dotted line is the approximation μ_{xa} given by Eq.(61).

Fig.(7) The longitudinal space-charge factor $\mu_z(A)$

Fig.(B.1) The transverse space-charge factors $\mu_x(A)$ for uniform charge distribution in a cylinder

Fig.(B.2) The longitudinal space-charge factors $\mu_z(A)$ for uniform charge distribution in a cylinder

Fig.(C.1) The transverse correlation factor $\mathcal{J}_x(A)$

Fig.(C.2) The longitudinal correlation factor $\bar{\mathcal{J}}_x(A)$

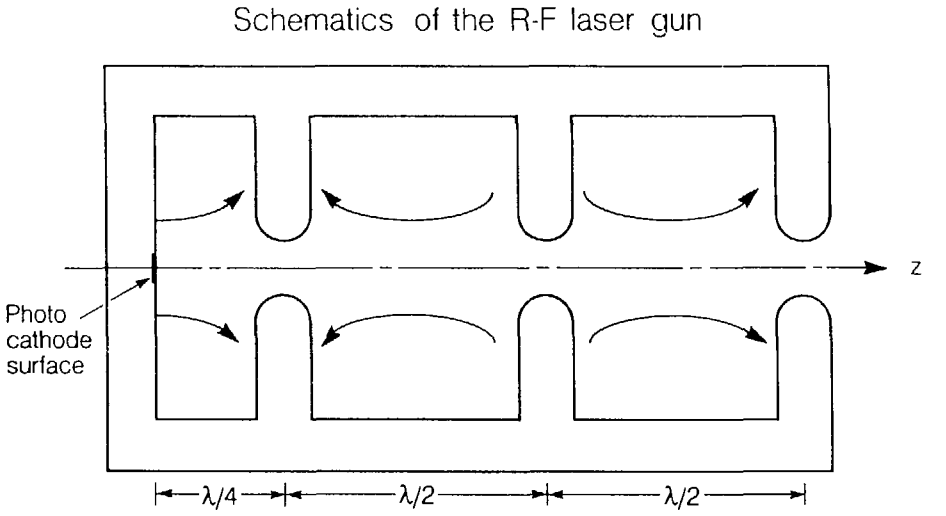

XBL 888-9264

Figure 1

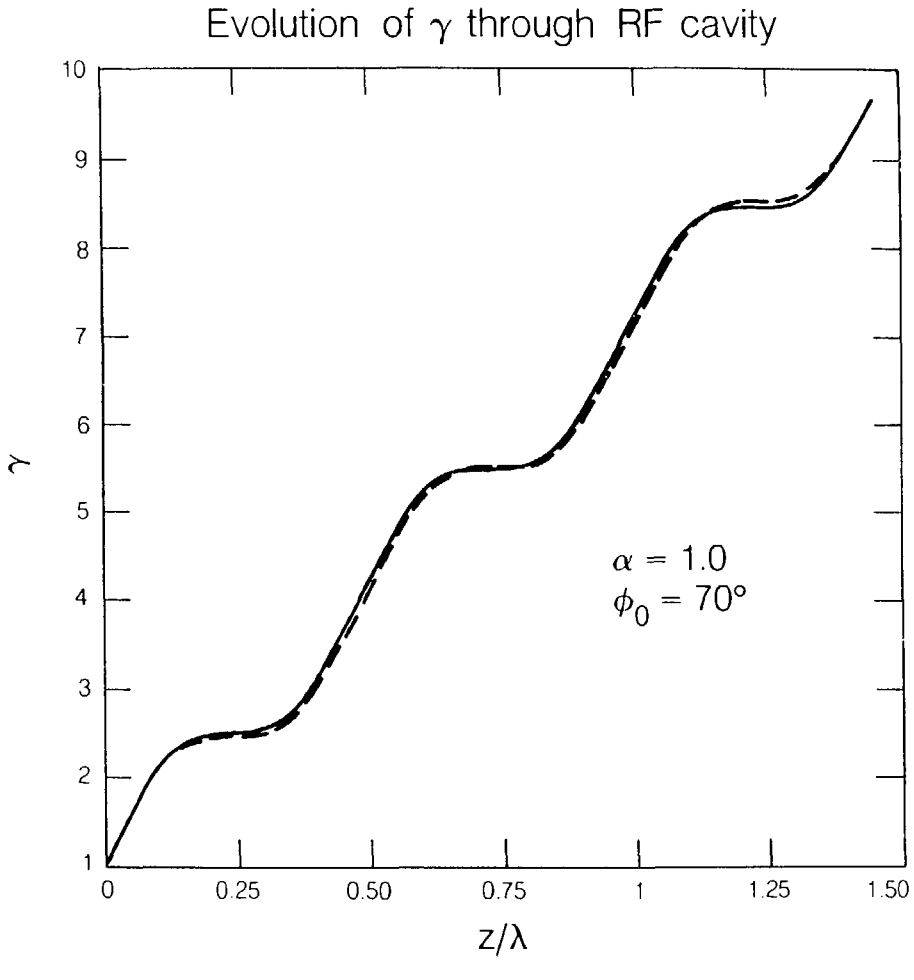

Figure 2(a)

XBL 888-9260

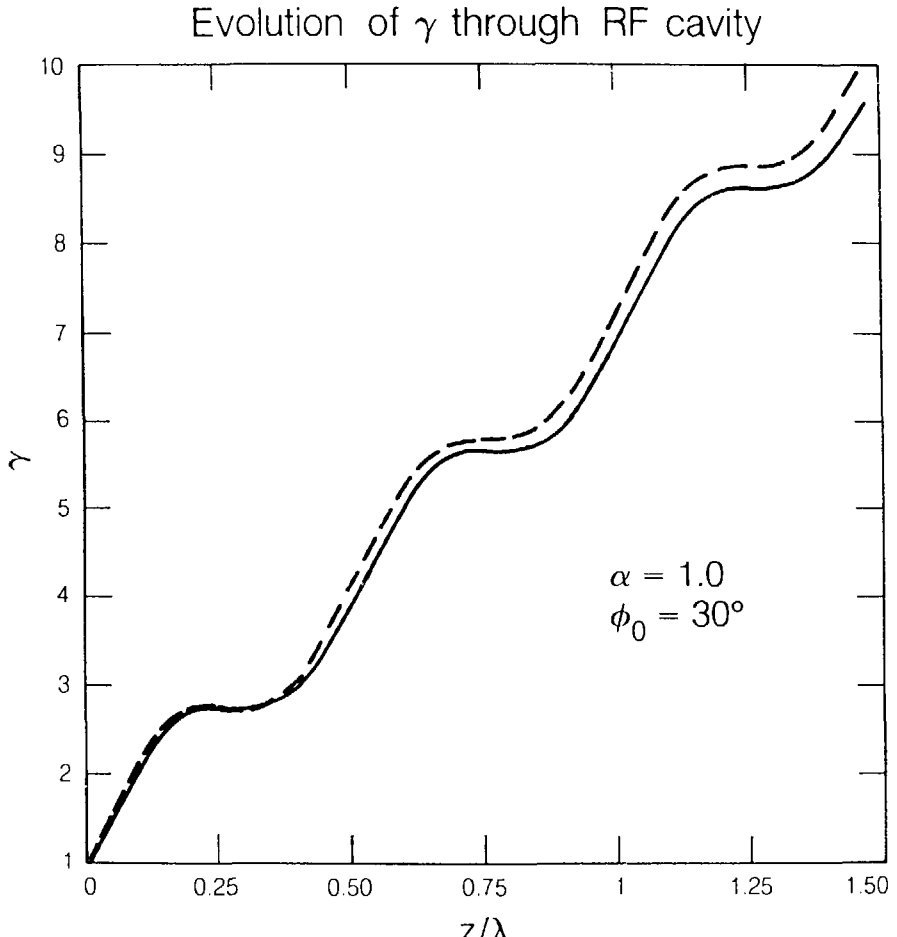

Figure 2(b)

XBL 888-9261

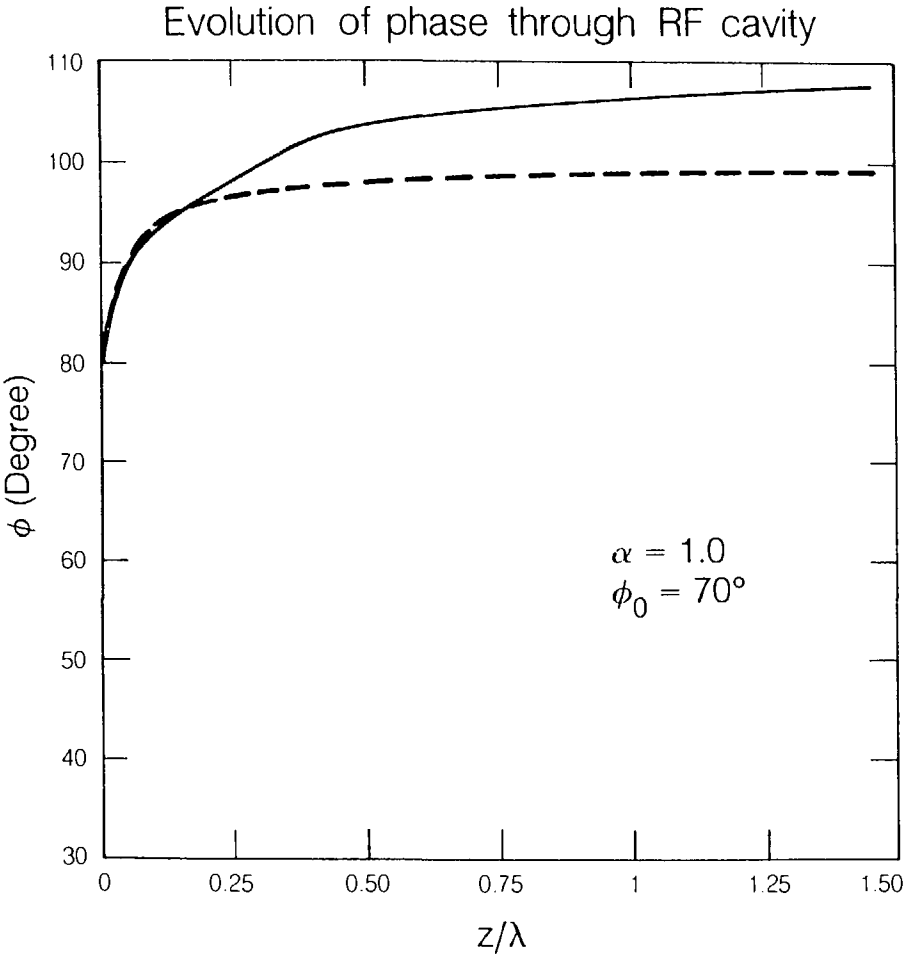

Figure 3(a)

XBL 888-9262

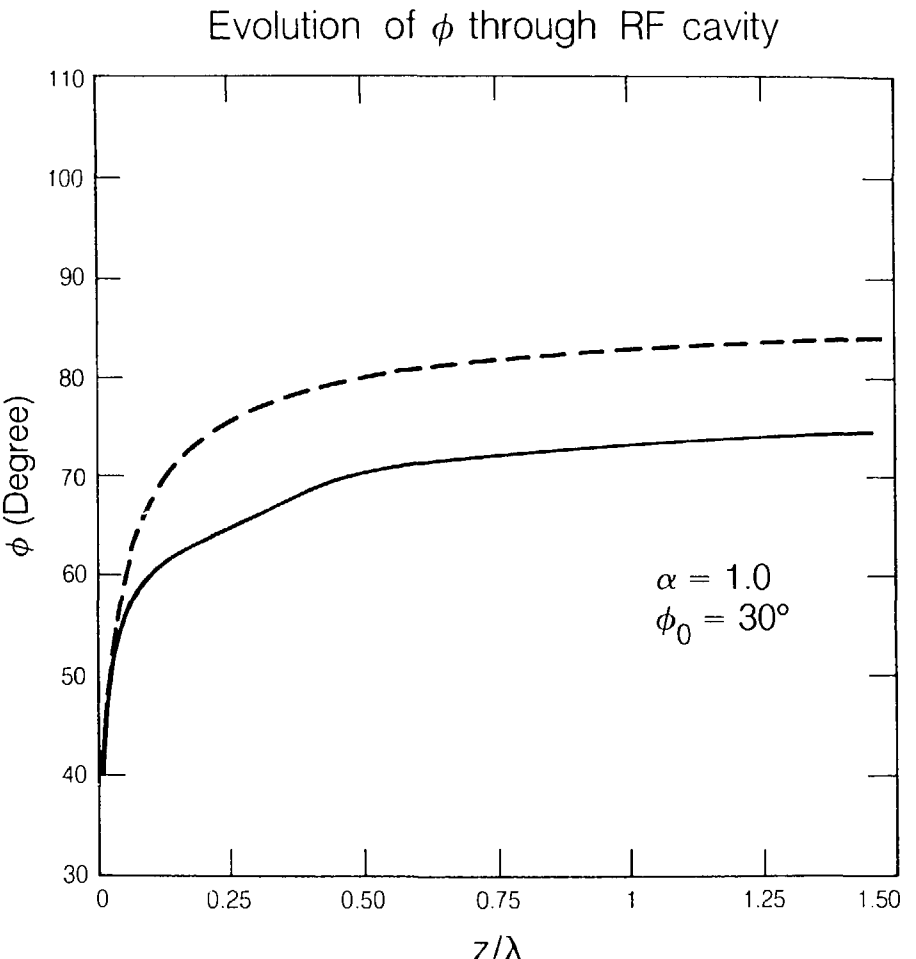

Figure 3(b)

XBL 888-9263

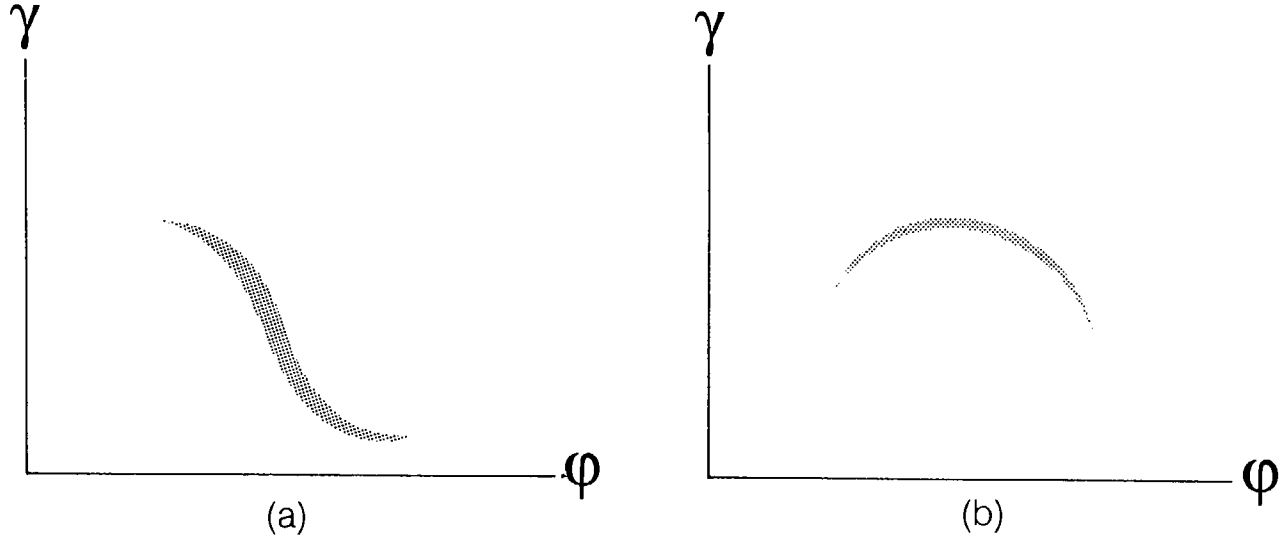

XBL 888-9252

Figure 4

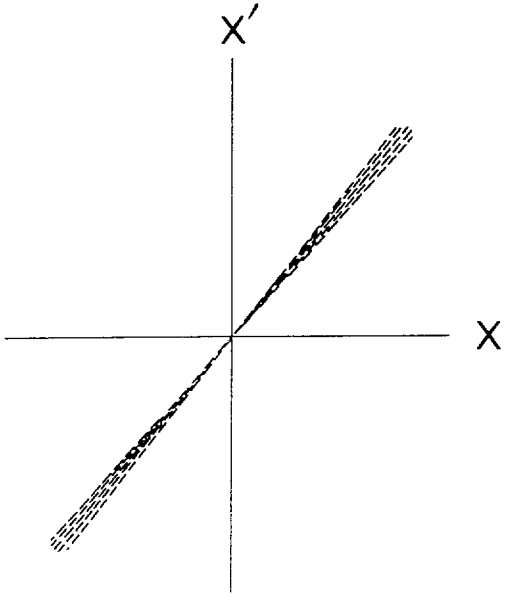

XBL 888-9253

Figure 5

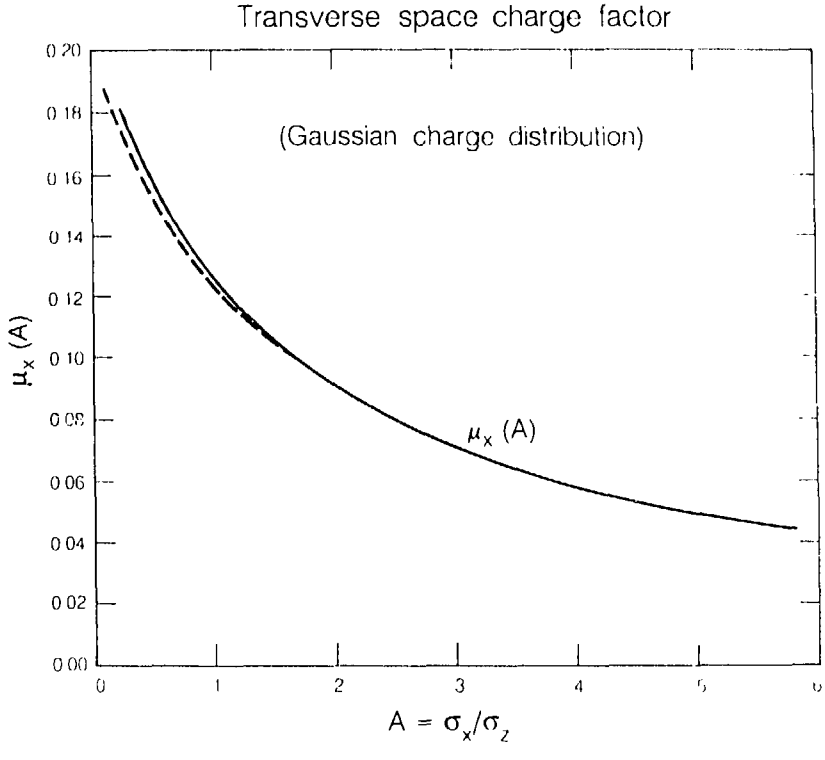

XBL 8885-4

Figure 6

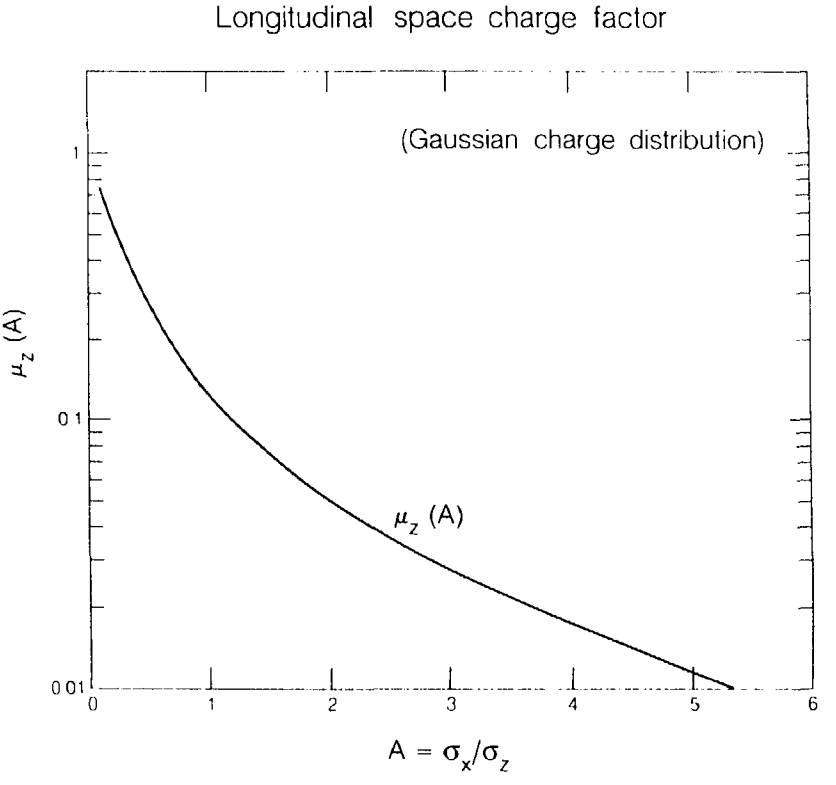
Longitudinal space charge factor
(Gaussian charge distribution)
μ_z (A)
μ_z (A)
1
0 1
0 01
0
1
2
3
4
5
6
A = σ_x/σ_z
XBL 888 9256

Figure 7

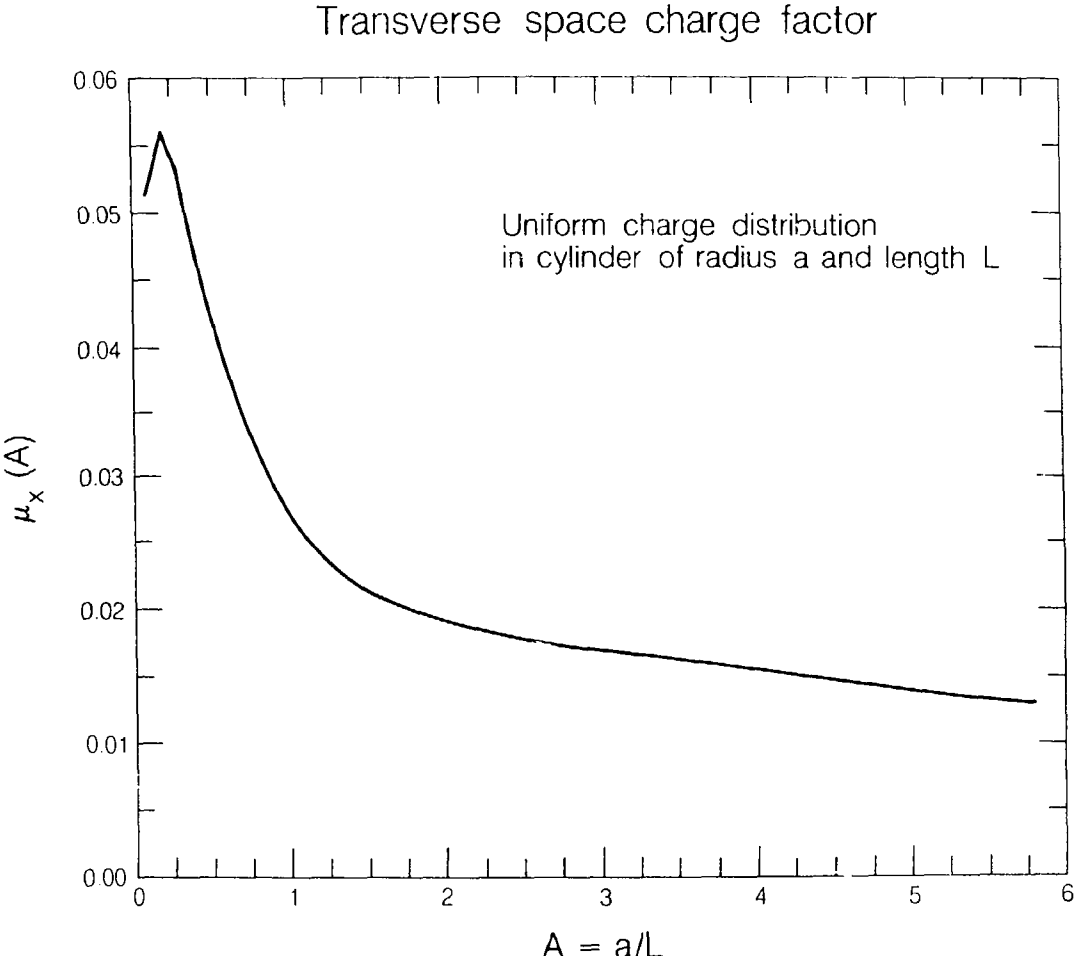

Figure B.1

XBL 888-9255

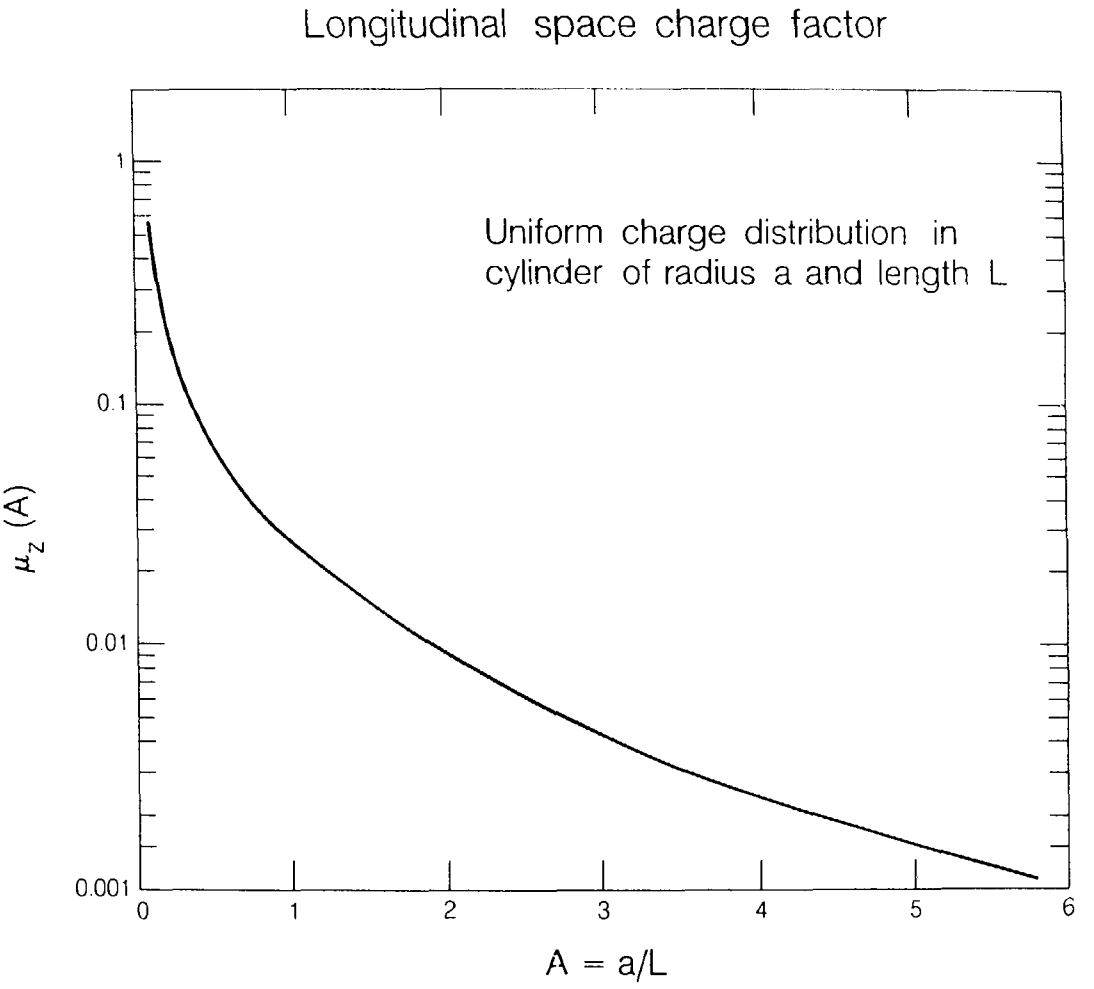

XBL 888-9257

Figure B.2

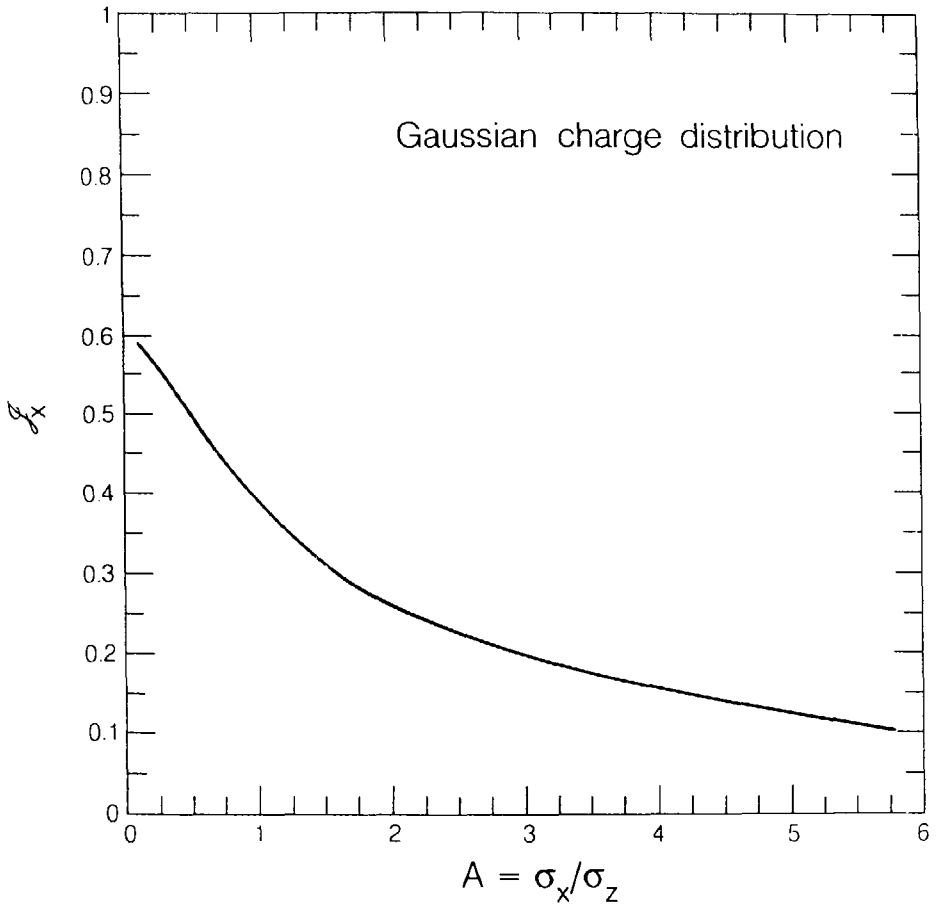

Figure C.1

XBL 888-9259

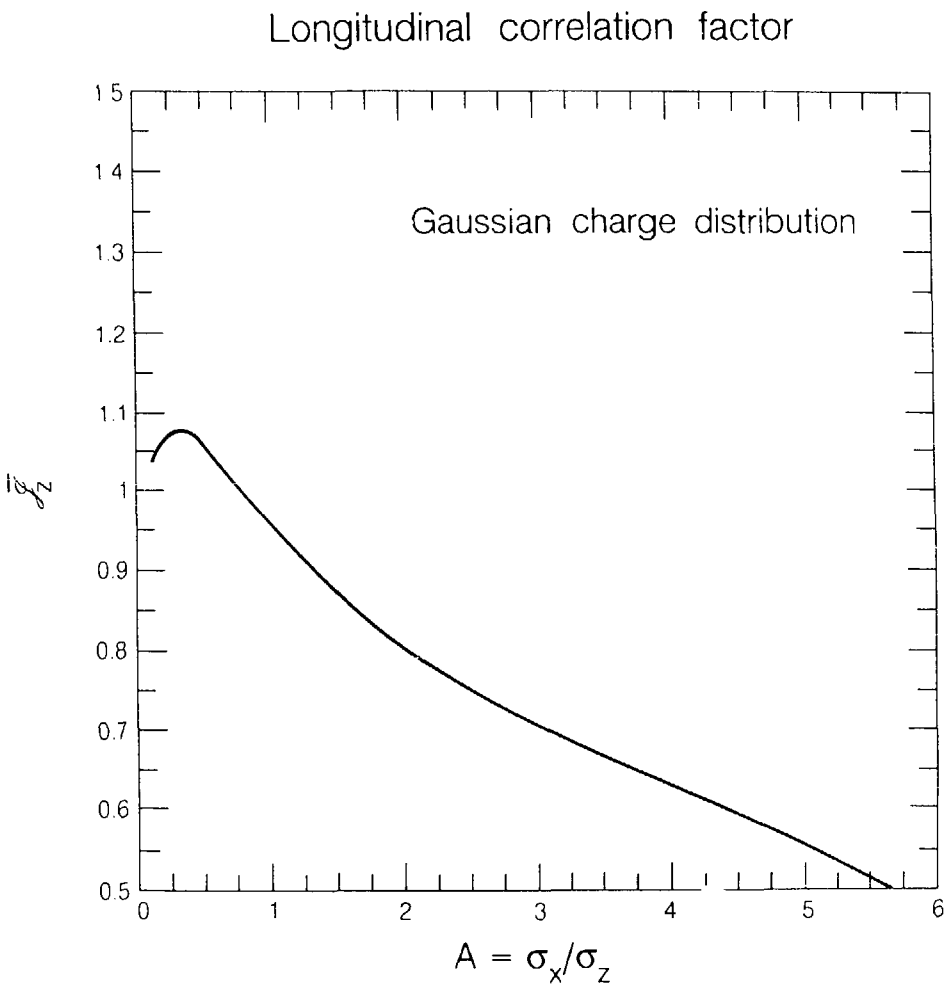

Figure C.2

XBL 888-9258